Anomalous Carrier Transport Model for Broadband Infrared Absorption in Metals

J. Orosco and C. F. M. Coimbra*
Department of Mechanical and Aerospace Engineering
Center for Energy Research
University of California San Diego
La Jolla, CA 92093-0411
(Dated: November 25, 2018)

We derive a model for accurately reproducing the broadband infrared optical response of common engineering metals. Here we use "broadband infrared" to refer to wavelengths beginning at 1 μm and extending to approximately 100 μm or more. The model generalizes the Drude theory to account for sources of anomalous intraband absorption. This is accomplished by modeling these sources as elements of disorder that introduce diffusive perturbations into the local field. In the stationary setting, the memory kernel description of the field relaxation leads to a fractional derivative with an order that corresponds to the memory decay strength. We demonstrate that this model is fully consistent with the Drude theory and that the semiclassical theory is recovered under requisite assumptions on the field relaxation or radiative wavelength. The anomalous model component is shown to reproduce empirically observed anomalous absorption that has been traditionally corrected by models possessing empirical components that have not been formally derived. Results are presented for several common metals for which the proposed model accurately reproduces the data over the entire modeled bandwidth. A comparative analysis confirms that the proposed model represents a robust, high fidelity alternative to previously proposed models that do not capture the observed physical response over the extended infrared range.

Keywords: Drude model, anomalous skin effect, Fermi liquid, conductivity, defect scattering, nonlocal effects

I. Introduction

The optical response of solid media subject to incident electromagnetic radiation is critical in a variety of commercial, industrial, and natural systems. Accurate determination of spectral properties is needed in order to meet the precise design requirements of modern devices [1, 2]. Practical characterizations of these responses commonly take the form of low-dimensional closed-form parameterizations of the relevant material property appearing in the Maxwell-Heaviside equations [3–5].

From a theoretical standpoint, closed-form models facilitate analysis and interpretation of the physical systems they embody. Closed-form models also address the need for compatibility with modern theoretical frameworks [6, 7]. In engineering applications, material response models are indispensable for the design and manufacture of optical and microelectronic devices. When combined with the Fresnel coefficients, these models further provide the means for estimation of the spectrally resolved radiative properties of the medium [8, 9].

When characterizing the optical response of metals, the essential property of interest is the macroscopic response of the average motion of free charge carriers in response to specific radiative forcing [10]. The intraband regime corresponding to this behavior resides approximately within the infrared spectral band for many metals of engineering interest. A reasonably accurate model for the free-carrier response of metals was originally proposed by Drude over a century ago [11]. Its popularity stems from the remarkable accuracy with which it predicts the experimental observations for many common metals despite its simple two-parameter structure. Due to its straightforward classical interpretation, the Drude model is often employed for the analysis of experimental data, as a starting point for the development of models that seek to extend its range of use, and as a baseline metric for the assessment of model performance [12–20]. Here we undertake an extension of the Drude model to account for anomalous intraband absorption by metals to broadband infrared radiative forcing. In this work, we use the phrase "broadband infrared" to refer to wavelengths beginning at 1 μm and extending to roughly 100 μm or more.

Despite its widespread use and simplicity, there are many situations in which the Drude model is insufficient to explain empirical data [13, 17, 21, 22]. To address some of these limitations in the intraband absorption by metals, we develop an anomalous model for the broadband infrared response. Engineering design applications requiring accurate models of the infrared optical response of metals are numerous and far-reaching, with use cases ranging from the development of nanoscale infrared antennas [18] to the design of structural IR signal suppression and mimicry technologies [23].

Our extended model is motivated by the results of our previous study [24]—as well as other studies indicating the need for such an extended framework [14, 15, 25]—and developed from the viewpoint that it should be useful when applied to the materials encountered in practical

* Corresponding author, ccoimbra@ucsd.edu

settings. It should therefore be capable of accurately reproducing anomalous absorption profiles that may arise at shorter wavelengths due to the presence of moderate surface imperfections or due to complicated valency configurations, along with other features not well described by the Drude model that tend to arise in the far infrared regime and that are intrinsic to the material. As a basis for assessing the model performance, we compare the results with those of the Drude and Drude-Roberts models. The Drude-Roberts model has been frequently used in the literature to achieve the same goals outlined here, although typically on a more limited bandwidth [8, 26]. It is the suitable choice for a comparative assessment with our model over the extended IR range and in the presence of the noted sources of anomalous absorption.

This work is organized as follows. In Sec. II, the anomalous conductivity model is derived from an equation of motion generalizing the standard Drude theory. This is used in the traditional way to arrive at expressions for the electric susceptibility and relative permittivity. The Drude-Roberts model is also defined and the relationships between the various models are briefly discussed. The properties of the proposed model are investigated in Sec. III within the formalism of our recently derived spectroscopic analysis framework [27]. Sec. IV provides a comparative analysis of the modeling results for several common metals. A brief discussion is given in Sec. V summarizing the main conclusions of the study.

II. Models

We use the term "anomalous" informally and without a specific quantitative definition. Rather, we use it to denote regimes of behavior that depart in some systematic manner from that predicted by the theory proposed by Drude. We will show that these anomalous behaviors are appropriately described by a non-integer order formulation that is often used to describe anomalous diffusion in the literature (see, *e.g.*, [28]).

A. Drude Model

The semiclassical Drude model for the intraband response of a bulk conductor to incident electromagnetic radiation is derived from the equation of motion for an individual electron (or more generally, for an individual charge carrier). Under a Langevin description, this has the form [29]

$$m^* \frac{dv(t)}{dt} + \zeta\, v(t) = e\,\mathcal{E}(t) + e\,\eta(t), \tag{1}$$

where v is the electron velocity, m^* is the effective mass, $\zeta = m^*/\tau_e$ is a phenomenological damping associated with velocity-randomizing scattering events occurring at an average rate $\gamma_e = 1/\tau_e$, and e is the elementary charge. The forcing is determined by the local field, which consists of the ordered component $\mathcal{E}$ and random fluctuations η. SI units are used throughout. Taking the ensemble average $\langle\,\cdot\,\rangle$ of the relevant quantities leads to a macroscopic description of the current density evolution:

$$\tau_e \frac{dj(t)}{dt} + j(t) = \frac{Ne^2\tau_e}{m^*}\,E(t), \tag{2}$$

where $\langle\eta\rangle = 0$, $\langle v\rangle = j/n\,e$, and $\langle\mathcal{E}\rangle = E$, and with n being the electron number density. Then under a Fourier transform, the frequency-dependent conductivity may be written:

$$\sigma_d(\omega) = \frac{\sigma_0}{1 - i\,\tau_e\,\omega}, \tag{3}$$

so that the DC conductivity is obtained as $\lim_{\omega\downarrow 0}\sigma_d(\omega) = \sigma_0 = n\,e^2\tau_e/m^*$. Having obtained the conductivity, the Drude susceptibility follows directly [30]:

$$\chi_d(\omega) = -\frac{\omega_p^2}{\omega\,(\omega + i\,\gamma_e)}, \tag{4}$$

where the plasma frequency is $\omega_p = \sqrt{n\,e^2/m^*\,\varepsilon_0}$ and ε_0 is the vacuum permittivity.

B. Drude-Roberts Model

Drude's earliest investigations into the optical properties of metals lead him to the definition of a two-carrier model of conductivity in 1900 [31–33]. It was not until four years later—in response to the prevailing theoretical mindset at the time—that Drude would abandon this idea in favor of (3), the latter being more commonly associated with his name [11]. Five decades later, Roberts reevaluated the utility of Drude's original model, defining the susceptibility (in our notation) [13]:

$$\chi_{dr}(\omega) = i\frac{\omega_{p,\infty}^2}{\omega\,\gamma_\infty} - \frac{1}{\omega}\left(\frac{\omega_{p,a}^2}{\omega + i\,\gamma_a} + \frac{\omega_{p,b}^2}{\omega + i\,\gamma_b}\right), \tag{5}$$

which we refer to in this work as the Drude-Roberts model. The first term in this model is an entirely empirical component that Roberts imposed in order to accurately fit experimental data for materials exhibiting an augmented absorption profile at energies just below onset. This term and its analogs have appeared frequently in the literature when fitting optical data [25, 26, 34, 35]. Its necessity is generally attributed to surface imperfections (surface roughness, oxidation, *etc.*).

Expression (5) implies the conductivity definition

$$\sigma_{dr}(\omega) = \sigma_\infty + \frac{\sigma_a}{1 - i\,\omega\,\tau_a} + \frac{\sigma_b}{1 - i\,\omega\,\tau_b}, \tag{6}$$

where the relation $\omega_{p,\infty}^2 = \sigma_\infty/\varepsilon_0\,\tau_\infty$ was arrived at by inferring a time constant $\tau_\infty = 1/\gamma_\infty$ in order to maintain dimensional consistency. This is necessitated by the fact that there is no time constant associated with the empirical susceptibility term in Roberts original definition (or

in any of the aforementioned references), though a time constant is implicit since his original definition is given in terms of the parameter σ_∞. Thèye has previously shown that even in well-treated samples, the structures modeled by the empirical term can be experimentally verified [25]. However, these structures can be made small if modern sample preparation techniques are employed that reduce to negligibility the surface roughness, and if the sample is completely unexposed to the environment until the moment of experimentation in order to mitigate the effects of surface contaminants [15].

C. Proposed Model

We take (1) as a starting point for our model derivation. Beginning in this way ensures that terms in the resulting response model have their origin in a corresponding equation of motion. In order to formulate a more complete model that accounts for microscopic anomalies in the local field that may result in macroscopically emergent anomalous dynamics, we consider a correction to (1) in the form of a generalized fluctuating field:

$$\widetilde{\eta}(t) = F\left(\mathcal{E}(t), \tau_f \frac{d\mathcal{E}(t)}{dt}\right) + \eta(t), \tag{7}$$

where τ_f may be regarded as a characteristic time of field relaxation. Since the zero-order field effect is already accounted for in the Drude model of (3), the simplest realization of the modified local field deviating from the Drude description is that which permits a Markovian relaxation $F = \tau_f \, d\mathcal{E}/dt$. A more general realization is one that accounts for the presence of a historical path-dependence, or memory, in the field damping:

$$\widetilde{\eta}(t) = \lim_{t_0 \downarrow -\infty} \int_{t_0}^{t} \mathcal{K}(t-s) \frac{d\mathcal{E}(s)}{ds} \, ds + \eta(t), \tag{8}$$

where it has been assumed that enough time has passed since "switching the field on" so that the initial distribution has been forgotten. The dimensionless function $\mathcal{K}$ is known as the memory kernel.

Our primary objective is that of obtaining a low dimensional description of the anomalous response that provides a general empirical fidelity while remaining amenable to physically meaningful interpretation. We motivate our choice of memory kernel accordingly and assess its practicality for the purposes of modeling and analysis further on. An appropriate choice is therefore

$$\mathcal{K}(t) = \frac{(\tau_f/t)^\mu}{\Gamma(1-\mu)}, \tag{9}$$

which imposes a power law memory decay. Here $\Gamma(\,\cdot\,)$ is the gamma (generalized factorial) function. The condition $\mu = 0$ implies a perfect memory. The limiting behavior of (9) in (8) as $\mu \to 1$ leads to the IID distribution $\mathcal{K}(t-s) \to \delta(t-s)$, which corresponds to the previously noted Markovian relaxation. For all values in between, an imperfect, decaying memory is implied, with the parameter $\mu \in [\,0, 1)$ determining the strength of decay.

With the specific choice of memory kernel given by (9), the improper integral on the right-hand side of (8) is equivalent to the stationary limit of either of the Riemann-Liouville or Caputo fractional derivative definitions [36]:

$$\lim_{t_0 \downarrow -\infty} \mathcal{K}(t) \ast \frac{d\mathcal{E}(t)}{dt} = \tau_f^\mu \frac{d^\mu \mathcal{E}(t)}{dt^\mu}, \tag{10}$$

where $\ast$ is the causal convolution operator. The interested reader is directed to Appendix A in the Appendix for a more general approach to the memory kernel that nonetheless leads to (10).

Due to their inherent infinite dimensionality, memory operators such as these find utility in the description of high-order semi-stochastic dynamics, which otherwise represent nondifferentiable processes. In Ref. [37] (and the references therein), nonlocal operators of the type used here are shown to be consistent with the Hamiltonian description of damping in many-body dynamics. The same cannot be stated about Markov approximations, which are frequently used for the description of anomalous diffusion processes. Thus, our model can be understood as describing the anomalous diffusion of field perturbations introduced by elements of system disorder. That is, application of a field impulse to the model system leads to relaxation processes in both the particle and the field, with the latter being described by a power-law decay. An analogous treatment applied directly to the electron using a generalized Langevin equation leads to an extended Drude model, a result that can be more rigorously achieved from quantum electrodynamics [38]. The memory function in this description possesses mathematical qualities similar to that of an electron self-energy [39].

Combining (8), (9), and (10), substituting into (1), and then taking the ensemble average, one has the macroscopic transport equation

$$\tau_e \frac{dj(t)}{dt} + j(t) = \sigma_0 \left(E(t) + \tau_f^\mu \frac{d^\mu E(t)}{dt^\mu}\right). \tag{11}$$

Before proceeding, we note that (11) is the statistical realization of a microscopic equation of motion that serves as a parsimonious analog to the equation of momentum for a spherical particle in unsteady fluid flows [40, 41]. This scenario gives rise to the Basset history drag, a force that is proportional to a half derivative on the disturbance field.

Following the same procedure previously used with the Drude expression, the carrier transport equation (11) leads to the susceptibility model

$$\chi(\omega) = \chi_d(\omega) + \chi_a(\omega), \tag{12}$$

where the anomalous contribution is

$$\chi_a(\omega) = -(-i)^{\mu}\frac{\omega_p^2}{\omega^{1-\mu}\,\gamma_f^{\mu}(\omega + i\,\alpha\,\gamma_e)}, \tag{13a}$$

$$= -\frac{\omega_p^2}{\omega^{1-\mu}\,\gamma_f^{\mu}}\left(\frac{f_r(\mu)}{\omega + i\,\alpha\,\gamma_e} + i\frac{f_i(\mu)}{\omega + i\,\alpha\,\gamma_e}\right), \tag{13b}$$

with $f_r(\mu) = \cos(\mu\,\pi/2)$ and $f_i(\mu) = -\sin(\mu\,\pi/2)$, so that

$$\sqrt{f_r(\mu)^2 + f_i(\mu)^2} = 1. \tag{14}$$

Expression (13b) shows that the effect of μ is to split the anomalous susceptibility into two separate terms. The relation (14) demonstrates that the strengths of the two terms—determined by $f_r(\mu)$ and $f_i(\mu)$—represent a complimentary partition of the overall energy of the anomalous contribution. This is made evident by considering the ratio of the two terms at a fixed frequency and as a function of μ, which is proportional to $f_i(\mu)/f_r(\mu)$. The energetic partitioning property of temporally nonlocal operators and systems when expressed in the frequency domain has been recently described in detail [27].

In expressions (13), the dimensionless parameter α allows the anomalous regime to be distinct from the Drude regime—for example, when the bulk interior response has a spectral onset that differs significantly from that of the admittance near the surface. The presence of this parameter represents a physical constraint that can be used to reduce the model complexity. It is motivated by considering a single effective carrier type having a time constant that may be modified by the factor α in the presence of secondary, anomalous structures.

Two important asymptotic characteristics of (12) should be noted: (i) in the limit of instantaneous field relaxation, $\tau_f \to 0$ and the proposed model reduces to the simple Drude expression (4), and (ii) in the limiting case of a DC field, $\omega \to 0$ and the corresponding conductivity model returns σ_0. Both of these conditions imply consistency with the underlying semiclassical theory. This level of consistency represents a benefit that is not available with the Drude-Roberts model.

With a susceptibility model in hand, the permittivity is expressed:

$$\varepsilon(\omega) = \varepsilon_\beta + \chi(\omega), \tag{15}$$

where the polarizability of the medium due to bound states,

$$\varepsilon_\beta = 1 + \lim_{\omega \downarrow 0}\sum_{\beta}\chi_\beta(\omega), \tag{16}$$

is typically either obtained by modeling the frequency-dependent bound electron contributions χ_β (using, *e.g.*, the Lorentz harmonic oscillator model) or in terms of the real constant obtained in the limit of (16). This is to say that if the intraband regime is the modeling focus and the interband dynamics are sufficiently decoupled from the free-carrier dynamics, then expression (16) is a valid approximation.

1. *Reduction of Model Complexity*

With respect to the Drude-Roberts model of (6), the proposed model structure in (13) is analogous to enforcing the constraint $\tau_b = \alpha\,\tau_a$, along with the assumption that the effective mass remains relatively constant, so that $\sigma_b = \alpha\,\sigma_a$. Frequently, we will realize models with $\alpha = 1$, so that the resulting single-pole-type structure implies a single time constant, with the Drude poles and the anomalous poles coinciding. In this case a parameter reduction is obtained without loss of accuracy.

The result of (13b) shows that the partitioning property of μ generates a secondary term. When combined, the the partitioned components serve a similar purpose to the empirical term in the Drude-Roberts model, except where now this behavior has been given a physical basis with an associated time constant. When $\mu = 1$, the anomalous term in the proposed model has a frequency dependence commensurate with that of the empirical term. With this in mind, we identify two simplified model structures. The first is the previously noted $\alpha = 1$ case, which leads to a four parameter model. If, in addition, $\mu = 1$, then one has the three parameter model

$$\chi(\omega) = -\frac{\omega_p^2}{\omega\,\gamma_e}\left(\frac{\omega\,\tau_f + 1}{\omega\,\tau_e + i}\right), \tag{17}$$

where we recall that $\gamma_e = 1/\tau_e$, and where it is again made obvious that one recovers the Drude model under the assumption of instantaneously diffusive field perturbations.

III. Model Physics

Since the Drude model is known to satisfy the Kramers-Kronig Relations (KKRs), the KKR consistency of the model represented in (12) and (15) is entirely dependent on the anomalous correction (13). This is so because the KKRs constitute a set of linear transforms when dealing with linear optical media [42]. An interesting result of the variable field damping memory is that two regimes of behavior must be considered when assessing the KKR consistency of the anomalous contribution. This can be most easily understood by considering the anomalous component of the model conductivity

$$\sigma_a(\omega) = i(-i)^{\mu}\frac{\sigma_0\,(\tau_f\,\omega)^{\mu}}{i + \omega\,\tau_e}, \tag{18}$$

where we have set $\alpha = 1$ without loss of generality.

When $\mu = 0$ the anomalous term reduces to a simple Drude term and therefore satisfies the KKRs for the susceptibility of conductive media. The second, less obvious regime occurs when $\mu \in (0, 1]$. In this regime, the anomalous conductivity component (18) vanishes in the low-frequency limit. In this case, the model is appropriately treated with the KKRs for dielectric media (as is necessary when assessing, *e.g.*, the Lorentz oscillator). In either of the foregoing cases, the response in (18) is

clearly holomorphic in the upper half plane so that Titchmarsh's theorem establishes causality. Here we have restricted our analysis to the principal Riemann sheet in order to avoid issues related to branch cuts generated by the fractional frequency term. Since the KKR consistency is readily obtained for $\mu = 0$ and $\mu = 1$ (where branch cuts vanish), and the damping remains nonzero for $\mu \in (0, 1)$, this restriction does not represent a loss in generality when establishing causality. The additional requirement of Hermicity follows from the fact that the response function was derived directly from a differential force balance.

In a recent study, we have derived a framework for the generalized spectroscopic analysis of frequency domain response dynamics [27]. The framework is derived within a variable order calculus formalism and leads to a variable order frequency response function. Within the context of the present study, the analysis framework has the form

$$\chi(\omega) = \frac{\omega_p^2}{\gamma(\omega)(-i\,\omega)^{q(\omega)}}, \tag{19}$$

where the frequency-dependent parameters γ and q—jointly referred to as the variable order coordinates (VOCs)—are the generalized damping and generalized derivative order, respectively. Setting $Z = \omega_p^2/\chi$, with $Z = Z' + i\,Z''$, the VOCs for the susceptibility can be solved for exactly:

$$q(\omega) = \frac{2}{\pi}\,\mathrm{atan2}(-Z''(\omega), Z'(\omega)), \tag{20a}$$

$$\gamma(\omega) = \omega^{-q(\omega)}|Z(\omega)|, \tag{20b}$$

where $|(\,\cdot\,)|$ is the complex modulus of $(\,\cdot\,)$ and with atan2 denoting the phase-sensitive arctangent function. The generalized derivative order reveals the most dominant internal forces as realized in the observed macroscopic response at a given frequency of incident radiation.

In the noted study, we have shown how the mathematical operators (fractional or integer order) in a differential force balance can be interpreted as defining a basis set for the complex-valued spectroscopic dynamic space. The material parameters (or coefficients) in the force balance then determine the unique trajectory taken by a dynamical system as it traverses the space. For second-order displacement differential equations—that is, the type that underly spectroscopic dynamics—the dynamic space may be divided into two regimes. When the forcing order (either corresponding to a given differential operator or to the response of the system) is within the interval $[0, 1]$, we use the designation "viscoelastic." When the forcing order is within the interval $[1, 2]$, we use the designation "viscoinertial." The interested reader is referred to Ref. [27] for more detail.

In Fig. 1(a), the susceptibility model of (12) has been plotted for aluminum. The model parameters are the same as those used further on in this work and were obtained using data from [43]. The generalized derivative order has been plotted in Fig. 1(b). In each of the plots, the Drude component and the anomalous component have also been plotted so that their energy-dependent contributions to the overall model can be separately assessed.

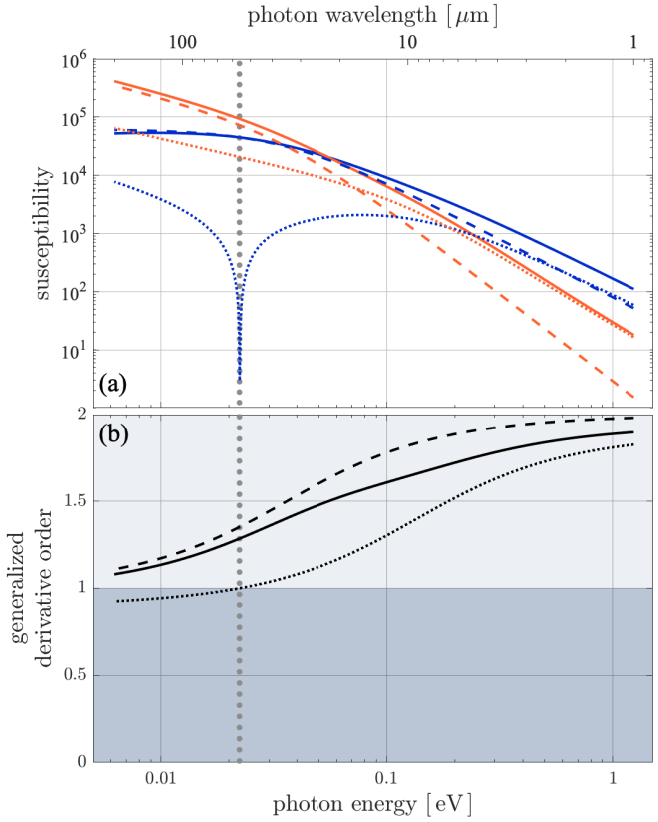

FIG. 1. Analysis of the aluminum susceptibility model (12) as a function of excitation energy, $\hbar\omega$. The parameters are taken from a model given in a later section of this work. In plot (a): $|-\mathbb{R}\mathrm{e}\{\chi\}|$ (dark, blue) and $\mathbb{I}\mathrm{m}\{\chi\}$ (light, orange) parts of the complete model (solid), the Drude component (long-dashed), and the anomalous contribution (short-dashed). In plot (b): frequency response of the generalized derivative order—as expressed in (20a) and derived in [27]—for the complete model (solid), the Drude component (long-dashed), and the anomalous component (short-dashed) over the viscoelastic (dark shaded) and viscoinertial (light shaded) regimes. The anomalous component represents a dissipative correction to the Drude component. The total model represents their combined effect. The vertical dotted line denotes the energy below which the anomalous component behaves as a quasi-bound state. In this regime, the anomalous term applies a positive correction to the negative real Drude susceptibility. This can be interpreted as disorder-based screening applied to the in-phase component of the overall polarization response.

A number of important insights can be extracted from the figure. At energies above $\approx 0.3\,\mathrm{eV}$, the real (dispersive) part of the anomalous term finds agreement with the Drude contribution, so that the two jointly determine the dispersion in this band. However, the overall

loss function is clearly a result of augmentation of the Drude contribution by the anomalous term, which manifests as the increase in absorption one typically associates with such features. In the plot of the generalized derivative order, one observes that the overall modeled response asymptotes to order 1 behavior at low frequencies (*i.e.*, when damping effects dominate) and asymptotes to order 2 behavior at higher frequencies (when inertial effects are important). This demonstrates that the viscoinertial $q \in (1, 2)$ regime corresponds to the free-carrier dynamics—as should be the case for a consistent analysis framework.

The plot of the energy-dependent derivative order confirms that the overall effect of the anomalous term is to apply a dissipative correction to the Drude contribution. This is expected given the tendency of such anomalies to increase absorption. Below $\approx 0.02\,\text{eV}$, the anomalous term exits the viscoinertial $q \in (1, 2)$ (*i.e.*, free-carrier) regime and enters the viscoelastic $q \in (0, 1)$ portion of a bound particle $q \in (0, 2)$ regime, remaining near the viscous boundary. This is directly related to the quasi-bound state behavior of the anomalous model component previously discussed and is the reason the bound oscillator KKRs must be used whenever $\mu > 0$ in (13).

To enable further characterization of the variable memory damping effect, the aluminum model is once more plotted in Fig. 2, except where now the analysis is limited to the complete model (12) and the memory decay parameter is taken over the range of values $\mu \in \{0, 0.2, 0.4, 0.6, 0.8, 1.0\}$. At larger μ, a second inflection develops in the absorption profile above $\approx 0.1\,\text{eV}$ representing augmentation of the absorptive dynamics in that band. This is precisely the behavior exhibited in, *e.g.*, the experimental data for silver used in a later section of the present study. In the monovalent noble metals, this type of early onset is generally attributed to imperfections in the sample surface such as defect scattering or thin films of oxidation [13, 15]. As μ is increased, the energy-dependent derivative order of the anomalous term—demonstrated in Fig. 1(b)—is shifted further into the viscoelastic regime. When $\mu = 1$, this curve resides entirely in this regime over the entire intraband region. As evidenced in Fig. 2(b), the complete model always resides in the free-carrier $q \in (1, 2)$ regime irrespective of the character of the anomalous component. For $\mu \gtrsim 0.5$, an inertial peak develops at $\approx 0.2\,\text{eV}$, beyond which the dynamics have an order that moves away from the conservative inertial boundary and toward the dissipative viscous boundary (corresponding to the early onset absorption).

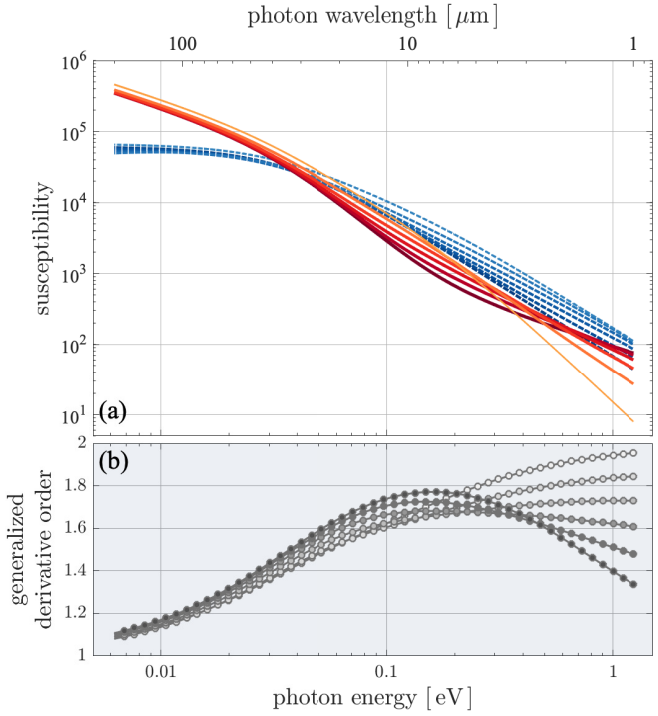

FIG. 2. Analysis of the aluminum susceptibility model (12) under tuning of the memory decay parameter, μ, and as a function of the excitation energy, $\hbar\omega$. The decay parameter is varied over $\mu \in \{0, 0.2, 0.4, 0.6, 0.8, 1.0\}$, with increasing value implying darker line colors in each plot. In plot (a): absorptive (solid) and dispersive (dashed) parts of the complete susceptibility model (12). In plot (b): frequency response of the generalized derivative order, as derived in [27]. When $\mu = 0$ (the lightest lines in each plot), the corresponding model is effectively that of a simple Drude oscillator. In this case, the low-energy dynamics are determined by the first order effects (since inertia has a much longer time to equilibrate in response to the forcing), whereas at higher energies the dynamics are determined by the second order inertial effects. For larger values of μ, an inertial peak develops above which the generalized derivative order moves away from the inertial boundary and toward the viscous boundary. This corresponds to the development of early onset absorption represented by the second inflection in the absorption profile (above $\approx 0.2\,\text{eV}$). This is also observed in, *e.g.*, the silver model and data given in a later section of this work. These effects are generally attributed to surface disorder in the experimental medium [13, 15].

IV. Empirical Fits to Optical Data

In this section we present a comparative analysis of modeling results for several common metals. Our choice is motivated by the conclusions of our earlier study [24], wherein a reductive optimal procedure was used to fit models to data for eleven metals over both the intraband and interband regimes, with the latter being expressed in terms of our recently developed bound oscillator model [5]. The results of [24] suggest that the model developed in the present study is apt for describing the infrared permittivity of aluminum, beryllium, silver, gold, and copper. Indeed, the model defined in this work accurately reproduces the data over a significantly extended spectral range, so that we have also found it meaningful to include modeling results for nickel.

TABLE I. Fixed model parameters. $\widetilde{\omega}_p$ is given in units of eV and ε_β is dimensionless.

	Al	Be	Ni	Ag	Au	Cu
$\widetilde{\omega}_p$	14.98	18.51	15.92	9.01	9.03	10.83
ε_β	18.77	15.50	1.01	2.35	5.37	5.51

A. Implementation

The plasma frequency $\widetilde{\omega}_p$ for each material can be found in the literature [1, 24]. These values are provided in Tbl. I. The best fit to each model is obtained by taking the oscillator strength definition with $\widetilde{\omega}_p$ fixed, as in the indicated references. The oscillator strengths are defined such that $\omega_p^2 = \widetilde{\omega}_p^2\, f_a$ for the Drude model, $(\omega_{p,\infty}^2/\gamma_\infty,\, \omega_{p,a}^2,\, \omega_{p,b}^2) = \widetilde{\omega}_p^2\,(f_\infty,\, f_a,\, f_b)$ for the Drude-Roberts model, and $\omega_p^2 = \widetilde{\omega}_p^2\, f_0$ for the proposed model. The oscillator strength f_∞ has been defined so that it absorbs the additional implicit γ_∞ factor. The interested reader can consult [24] for greater detail.

The parameters for each model were obtained by minimization of the standard model-fitting objective

$$\mathcal{V}(\theta) = \sum_{m=1}^{M} \left(|\Delta_r(\omega_m;\theta)| + |\Delta_i(\omega_m;\theta)|\right)^2, \tag{21}$$

with the relative error residuals defined such that

$$\Delta_i(\omega_m;\theta) = (\varepsilon''(\omega_m;\theta) - \varepsilon''_m)/\varepsilon''_m, \tag{22a}$$
$$\Delta_r(\omega_m;\theta) = (\varepsilon'(\omega_m;\theta) - \varepsilon'_m)/\varepsilon'_m, \tag{22b}$$

and where $\varepsilon(\omega;\theta) = \varepsilon'(\omega;\theta) + i\,\varepsilon''(\omega;\theta)$ defines the model evaluated at frequency ω given a parameter set θ. The experimental data, $\varepsilon_m = \varepsilon'_m + i\,\varepsilon''_m$, is defined on the M-sized frequency grid ω_m, with $m \in [1, M]$. Initial minimization of (21) was achieved by using a swarm intelligence method known as the Grey Wolf Optimizer to obtain a "global" minimum [44]. The result was then refined using the method described in [24]. Prior to optimization, the grid was scaled in accordance with conclusions of Pintelon and Kollár in [45]. A byproduct of that study is the result that the noted scaling method is also appropriate for models having a noninteger order grid dependence (as is so for the proposed model).

The bound state contribution to the electronic polarizability of each medium is recovered in the limit of (16) applied to the interband portion of the respective models obtained in our previous study [24]. These calculated values are included with the plasma frequency for each metal in Tbl. I. In the cases of beryllium and nickel, a significantly improved fit to all model structures was obtained by optimizing the traditional Drude expression with $\varepsilon_\beta \geqslant 1$ taken as a free parameter, and then the fixing the resulting values when fitting the remaining models.

B. Analysis of Results and Discussion

The models for each material were obtained from sources well established in the literature [43, 46–48]. The results are plotted in Figs. 3–8 for aluminum, beryllium, nickel, silver, gold, and copper, respectively. The parameter sets and associated errors for the proposed model are given in Tbl. II, whereas those for the Drude and Drude-Roberts models are provided in Tbl. III. Both the Drude-Roberts and proposed models represent a substantial, across the board improvement over the Drude model. This is generally the case due to an improved fit at non-intermediate wavelengths.

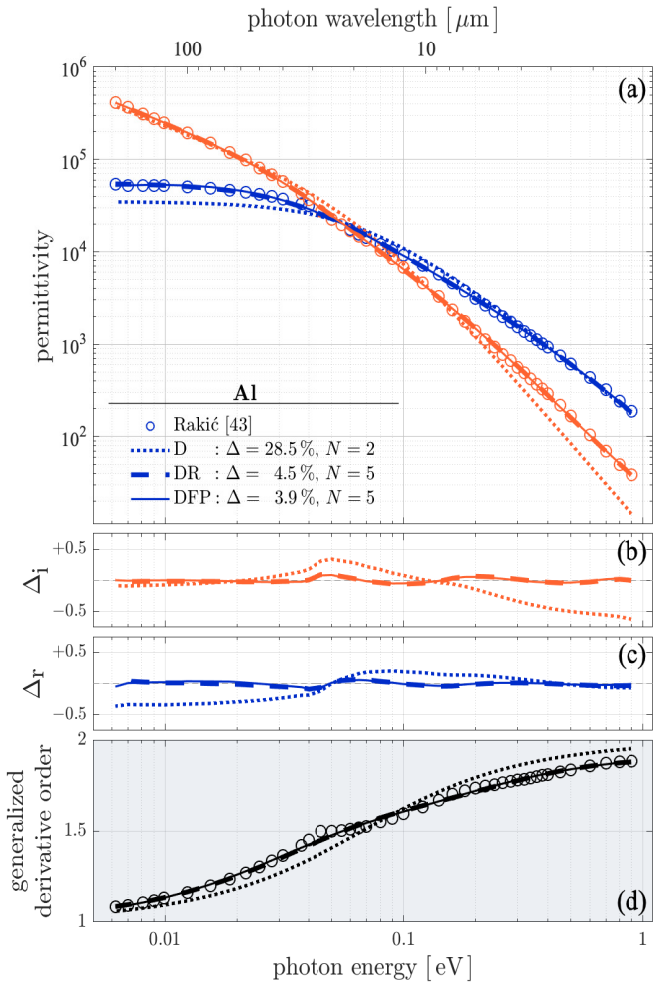

FIG. 3. Permittivity of aluminum. In plot (a): ε'' (light, orange) and $-\varepsilon'$ (dark, blue) given in terms of experimental data (markers) and models (lines). N denotes the number of parameters used in the respective model. The Drude (D) and Drude-Roberts (DR) model parameter values are given in Tbl. III. We refer to the model in the plot as the diffusive field perturbation (DFP) model. The proposed model parameter values are provided in Tbl. II. The residual subplots (b) and (c) are in terms of (22) and the energy-dependent derivative order in plot (d) is defined in (20a).

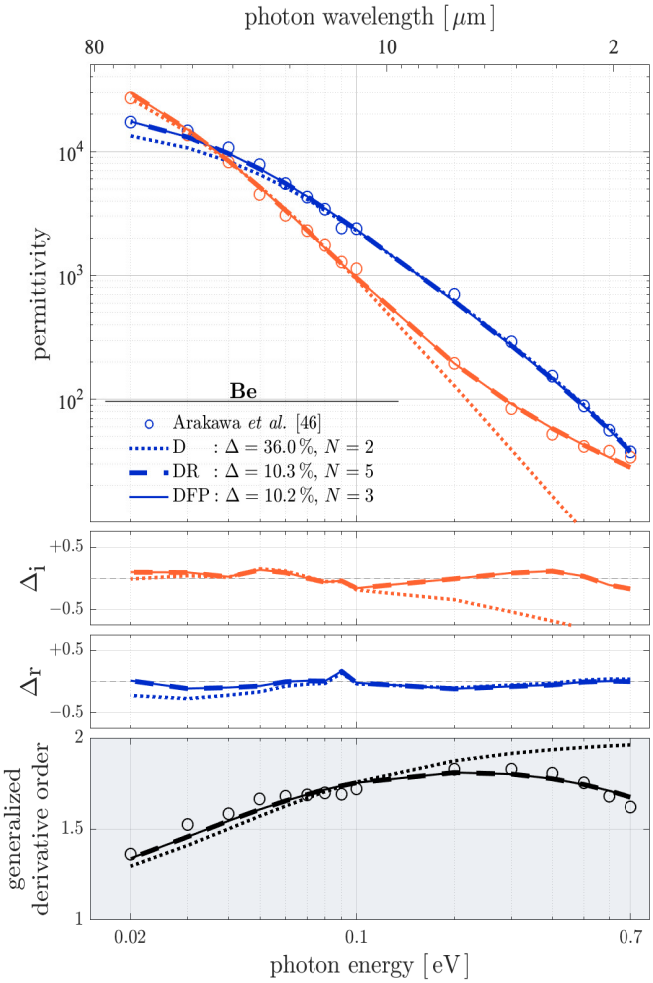

FIG. 4. The same as Fig. 3, except for beryllium.

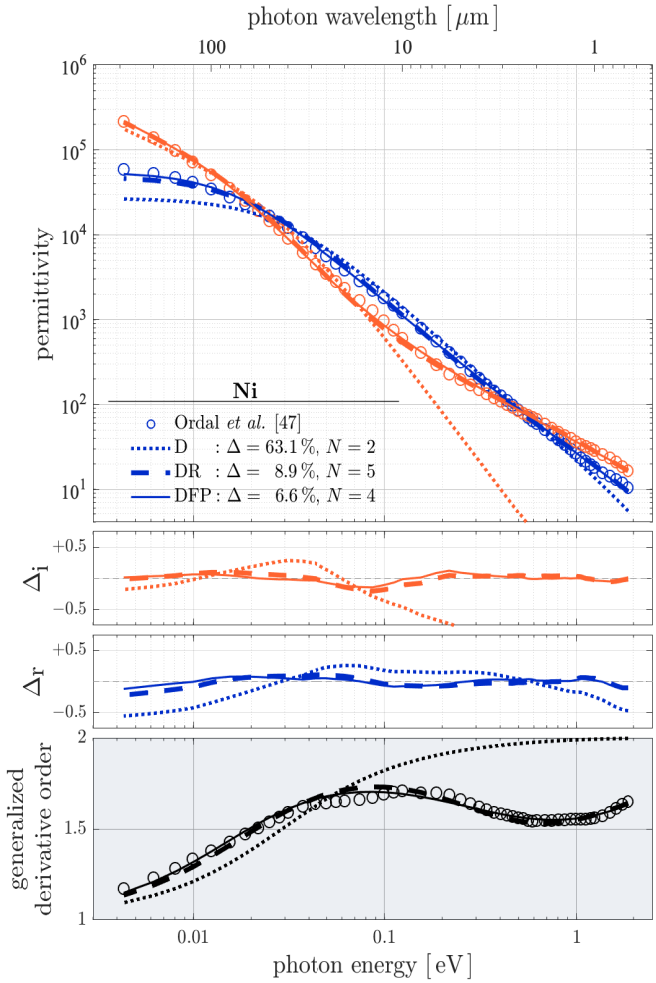

FIG. 5. The same as Fig. 3, except for nickel.

TABLE II. Parameters for the proposed model. γ_e is given in units of eV and γ_f^μ is given in units of eV$^\mu$. All others dimensionless. Blank entries for μ and α denote unity (*i.e.*, not a structural parameter).

	Al	Be	Ni	Ag	Au	Cu
f_0	0.357	0.078	0.063	1.042	0.928	0.646
γ_e	0.036	0.033	0.016	0.021	0.043	0.095
γ_f^μ	0.862	1.482	0.420	21.277	12.195	35.714
μ	0.105		0.788		0.187	0.373
α	3.721				0.098	0.026
% Δ	4.0	10.2	6.6	7.0	4.5	5.8

For the monovalent noble metals (Figs. 6–8), the small-wavelength deviation is mainly due to the previously noted increase in absorption typically associated with surface imperfections. In the absence of such imperfections, these materials are expected to remain linear (in log-log space) up to the onset energy E_0 [14, 15]. In the case of nickel (Fig. 5), the source of this excess absorption is partially due to the more complicated valency structure. Theoretical band calculations for nickel—which has the electron configuration [Ar] $3d^8\,4s^2$—predict structure near $\hbar\omega \approx 0.8\,\text{eV}$ due to interaction from the lower lying d-orbital valencies [49], which remain dormant at lower energies. Although this is not readily observed in the corresponding permittivity plot, it is immediately apparent by inspection of the generalized derivative order subplot, where a dissipative minimum is centered about the expected spectral coordinate. We note that these dynamics are reproduced by the proposed model with high-fidelity over the broad band 0.67–286 μm in one less parameter than the Drude-Roberts model. The proposed model has a relative percent error of just 6.6 % over this band, which represents an order of magnitude improvement over the Drude model.

A small part of beryllium's excess small-wavelength absorption is due to overlap from the broad interband behavior at $\hbar\omega \approx 3\,\text{eV}$ (outside the modeled band), which

TABLE III. Parameters for the Drude and Drude-Roberts models. γ_a and γ_b are given in units of eV. f_∞ is given in units of eV^{-1}. All others dimensionless.

	Drude						Drude-Roberts					
	Al	Be	Ni	Ag	Au	Cu	Al	Be	Ni	Ag	Au	Cu
f_a	0.705	0.078	0.090	1.040	1.007	0.659	0.380	0.076	0.069	1.040	0.997	0.318
γ_a	0.067	0.040	0.029	0.023	0.043	0.097	0.040	0.033	0.019	0.021	0.041	0.067
f_b							0.363	0.026	0.104	0.050	0.062	0.340
γ_b							0.192	8.256	1.208	9.982	6.185	0.123
f_∞							0.053	0.049	0.095	0.044	0.012	0.007
% Δ	28.5	36.0	63.1	32.2	15.7	15.7	4.5	10.3	8.9	7.0	9.3	10.2

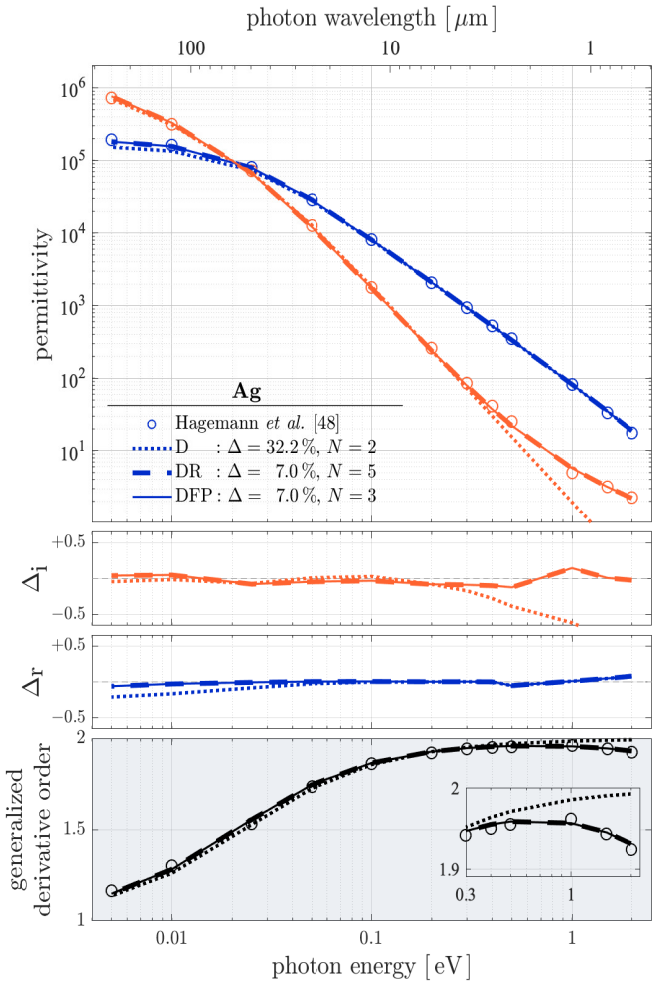

FIG. 6. The same as Fig. 3, except for silver.

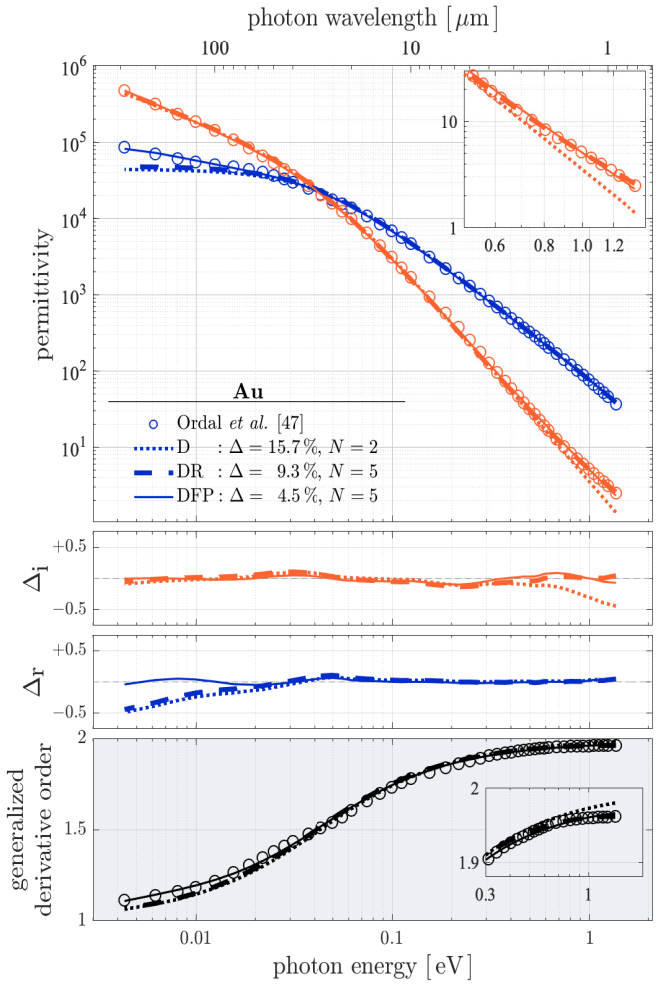

FIG. 7. The same as Fig. 3, except for gold.

is predicted by band theoretical calculations [50] and empirically supported by modeling experimental data, as in our previous study [24]. However, we note that our previous study directly modeled interband dynamics through a reductive algorithm and that this algorithm not only removed physically unjustified interband oscillators, but also specifically selected for a secondary Drude-like mechanism on the same data used in the present work. Thus, we consider this range to be valid application of the model.

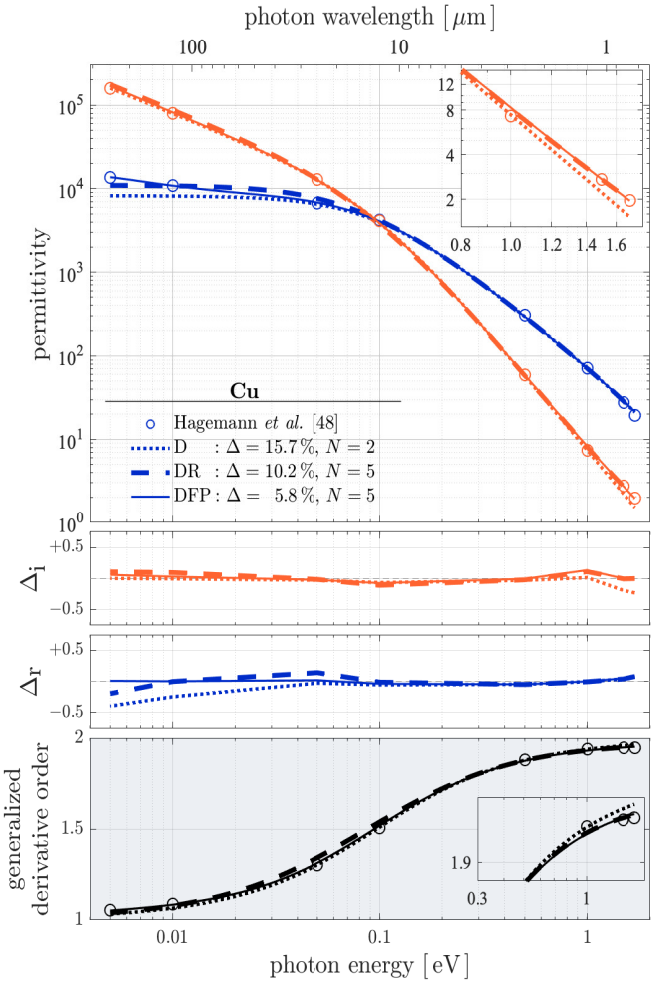

FIG. 8. The same as Fig. 3, except for copper.

The modeling results for aluminum (Fig. 3) indicate that proposed model yields a slight improvement over the Drude-Roberts model, and roughly one order of magnitude improvement over the Drude model. Comparison of the permittivity plot with that of the generalized derivative order leads to the observation that at longer wavelengths, the Drude model tends to overestimate the dissipative effect of the medium due to underestimating the in-phase response. At smaller wavelengths, the opposite is true as the Drude model overestimates the tendency of the system to reject energy due to underestimating the electronic absorption. Similar features—augmented by the effects of surface imperfections—are observed in the models for the noble metals. This is especially the case at longer wavelengths, where the Drude-Roberts model struggles to accurately track the data.

One well-known source of deviations from strict Drude description is the effect of electron-electron interactions [25]. Gurzhi has shown that, under a linearization of his quantum electron transport equation, Landau's Fermi liquid formalism implies a contributions to the effective collision rate having a quadratic dependence on the incident field [51, 52]:

$$\gamma_{ee}(\omega) = \gamma_{ee}(0)\left[1 + \left(\frac{\hbar\,\omega}{2\,\pi\,k_b\,T}\right)^2\right], \tag{23}$$

where $\gamma_{ee}(0) = \omega_p(k_b\,T/\hbar\,\omega_p)^2$, for a medium of temperature T and with k_b being Boltzmann's constant [25]. The result was derived under the assumption that $\hbar\,\omega$, $k_b\,T$, and $k_b\,\Theta_D$ (Θ_D is the Debye temperature) are all much less than the Fermi energy, E_F. This result also assumes NIR wavelengths, which Gurzhi defined as $\lambda \in [1, 10]$ μm. In an effort to reconcile these behaviors, Thèye [25] has previously applied an analysis to gold that is similar to a more recent technique known as the extended Drude analysis [16, 21]. This involves separating the real and imaginary parts of the Drude permittivity (15) in terms of (4), and then solving for a frequency-dependent time constant:

$$\tau(\omega) = \frac{\varepsilon_\beta - \varepsilon'(\omega)}{\omega\,\varepsilon''(\omega)}, \tag{24}$$

where ε_β is estimated from (16). Then the frequency dependent collision rate is $\gamma(\omega) = 1/\tau(\omega)$.

We find this variable time constant analysis framework useful here for describing the range of dominance of the quadratic collision rate dependence and for interpreting the limitations of each model structure. For this reason, we extend Thèye's analysis to the broadband infrared response of gold as represented by the room temperature data of Ordal *et al.* [47]. Due to the similar valency structure of the noble metals, and owing to the similar performance of the models on these materials, this analysis provides insight extending to the results of all three. The corresponding relevant values are: $k_b\,T \approx 0.0257$ eV, $k_b\,\Theta_D \approx 0.0153$ eV, and $E_F = 5.5$ eV, so that we expect (23) to remain valid (though not necessarily dominant) for the full NIR range defined by Gurzhi. The results of this analysis are presented in Fig. 9.

It is a common practice to evaluate the presence of γ_{ee} by plotting the collision rate against a quadratic energy grid [15, 21, 25], as we have done in Fig. 9(a). In this plot, the region of dominance of (23) is made immediately apparent. It is also apparent that the Drude-Roberts model very accurately describes this behavior. Within the present context, however, such a plot can be misleading, as the squared grid has the opposite effect of a more traditional logarithmic axis and we have modeled over a broadband infrared regime. In order to resolve this issue, we have plotted the equivalent relation $\gamma(\omega)\,/\,\omega = 1\,/\,\omega\,\tau(\omega)$ against $\hbar\,\omega$ in the inset of Fig. 9(a), which then permits the use of a log-log scaling. The electron-electron dominant regime $\hbar\,\omega \in [0.4, 1.4]$ eV remains intact, but it is now made apparent that this constitutes a very small portion, $\lambda \in [0.89, 3.10]$ μm, of the total modeled band, $\lambda \in [0.91, 286]$ μm, the latter part of which both the Drude and Drude-Roberts models fail to accurately track.

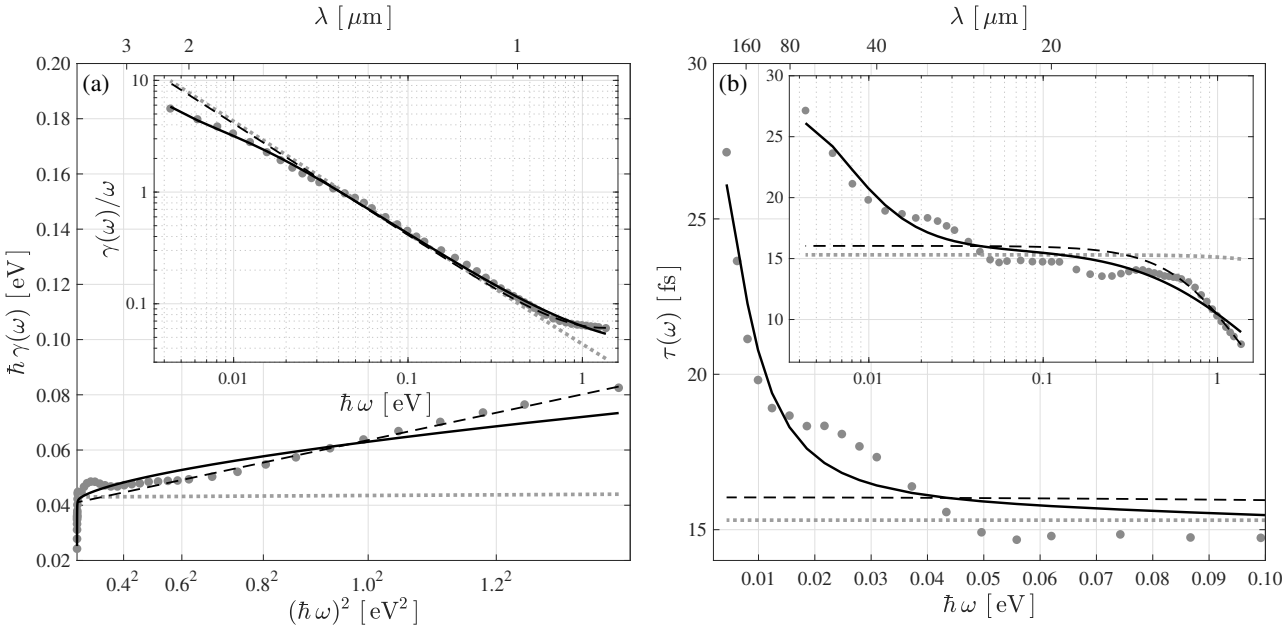

FIG. 9. Extended Drude analysis [16, 21] of the gold permittivity data [47] and corresponding models from Fig. 7. In each plot: data (gray dots), Drude model (dashed gray line), Drude-Roberts model (dashed black line), and proposed model (solid black line). The linear portion of the data in plot (a) indicates the regime over which electron-electron effects dominate in accordance with (23). The log-log inset of plot (a) was obtained by dividing both sides of Gurzhi's relation by $\hbar\omega$ in order to restore the direct $\hbar\omega$ dependence. Plot (b) demonstrates a high level of agreement with recent results [15], which were collected from carefully treated samples in order to eliminate the effects of surface imperfections. The units of plot (b) are angular femtoseconds, so that a direct comparison can be made with that study. The inset of plot (b) demonstrates that the proposed model provides a general fidelity over the entire bandwidth of the data.

Although the proposed model does not produce the same slope in the electron-electron dominant regime on the quadratic grid in Fig. 9(a), it nonetheless predicts the linearity (*i.e.*, the quadratic dependence) and also accurately describes the permittivity of the sample along this band (see inset of Fig. 7). This band corresponds directly to the anomalous absorption due to surface defects and, as indicated by the previous discussion, these effects are not included in the derivation of (23). One further notes that the proposed model has provided a modeling fidelity for the noble metals that either meets or exceeds that of the Drude-Roberts model. In the case of silver, this has been accomplished using the reduced complexity model of (17) (*i.e.*, with two fewer parameters than the Drude-Roberts model), while still accurately capturing the full bandwidth of the permittivity data $\lambda \in [0.62, 248]$ μm. A similar result was also obtained for beryllium.

We have expanded on the previous analysis by plotting $\tau(\omega)$ against $\hbar\omega$ in Fig. 9(b) and on a log-log scaling in the inset. This makes it clear that the $\tau(\omega)$ implied by the proposed model approximately describes the behavior over the *entire* bandwidth of the data. Furthermore, the Drude-Roberts model appears to asymptote to a constant value of $\tau(\omega)$ at lower frequencies, which is precisely the behavior of (23) in the DC limit. It is a critical observation that the results described in the plot are in good agreement with those obtained outside of experimental uncertainty from the same analysis performed in a recent study [15]. In that study, the experimental samples have been produced by a modern technique that reduces the RMS surface roughness to the order of 1 nm. Furthermore, they have isolated the samples from the environment until the moment of experimentation, so that anomalous absorption has been reduced to negligibility. In other words, the results described in Fig. 9 represent general behaviors that are intrinsic to the material.

V. Concluding Summary

The optical properties of metals subject to incident radiative forcing are largely determined by the average motions of their charge carriers. For the broadband infrared regime corresponding to wavelengths greater than roughly 1 μm, the responses of many metals and alloys commonly used in engineering applications are dominated by the intraband transitions of their free charge carriers. The standard model for these behaviors is that given by Drude over a century ago. Due to its relatively simple structure, its classical interpretation, and its general empirical fidelity, the Drude model remains in common use in both research and applied contexts.

However, in many practical circumstances involving

the design of photonic devices, the Drude model is insufficient for accurately reproducing the optical response of commonly used metals. This is observed even in media that are expected to be well described by the Drude theory, such as the monovalent noble metals. At shorter infrared wavelengths, anomalous absorption often arises due to the presence of surface imperfections that are ubiquituous in practical settings (*i.e.*, those occurring outside of meticulously controlled experimental conditions). At both short and long wavelengths, other effects that are innate to the medium—nontrivial valency structure, electron-electron interactions, anomalous skin effects, *etc.*—may play an important role and lead to a systematic divergence from the Drude model. Thus, accurately reproducing the broadband infrared response of metals common to engineering applications requires more flexible and robust models.

In this work, the Drude model has been generalized to account for the effects of anomalous features by modeling their presence as diffusive perturbations in the local field. To account for the semi-stochastic nature of these perturbations, a generalized memory kernel is assumed that leads, in the stationary setting, to a fractional derivative having an order of differentiation corresponding to the perturbation memory decay strength. We show that this generalized response model is consistent with the semi-classical Drude theory, reducing to the standard model under anticipated conditions. Namely, when the characteristic time of field relaxation approaches zero or in the long-wavelength limit.

When the field relaxation time is nonzero, the anomalous portion of the proposed model bifurcates, generating a secondary term that contributes directly to an anomalous absorption profile. It is demonstrated that the bifurcation represents a partitioning of oscillator energy into the anomalous absorption component. This anomalous absorption profile has been empirically confirmed in numerous studies and is observed in most practical settings. This behavior is traditionally modeled in the literature by empirical means lacking well-defined physical explanation. Under prescribed conditions, two simplified versions of the proposed model are identified that permit a reduction of model complexity (*i.e.*, fewer structural parameters).

Parameterizations of the proposed model have been obtained for several metals over broadband infrared regimes. The selected metals, which are commonly used in engineering applications, exhibit anomalous features and are not well described by the Drude theory. A comparative analysis of the proposed model results is facilitated with fits to both the Drude model and to the Drude-Roberts model. The latter was selected for its competitive modeling fidelity, though the higher fidelity is only achieved with the inclusion of empirical model components lacking a formally derived origin. The analysis has revealed that the Drude model tends to perform well only at intermediate wavelengths and that the Drude-Roberts model struggles to accurately track the data at long wavelengths. The model proposed in this works meets or exceeds the fidelity of both comparison models in all cases, and typically introduces fewer additional parameters than the Drude-Roberts model. A variable Drude time constant analysis reveals that the proposed model implies a frequency-dependent time constant that more completely describes the data over the entire modeled bandwidth.

A. Stationary Character of the Stretched Mittag-Leffler Memory Decay

The stretched Mittag-Leffler (SML) decay,

$$E_\mu(-(t/\tau_f)^\mu) = \sum_{n=0}^{\infty} \frac{(-(t/\tau_f)^\mu)^n}{\Gamma(\mu\, n+1)}, \tag{A1}$$

is a hybridization of the Mittag-Leffler function with the stretched exponential relaxation implied by the Kohlrausch-Williams-Watts (KWW) response model [53–55]. The SML decay represents a generalization of the traditional exponential decay in the sense that for $\mu = 1$, one recovers $\exp(-t/\tau_f)$, as can be verified by inspection of (A1). For finite τ_f, the SML achieves a scaled power-law dependence in the stationary limit [55]:

$$\lim_{t\uparrow\infty} E_\mu(-(t/\tau_f)^\mu) = \frac{(t/\tau_f)^{-\mu}}{\Gamma(1-\mu)}, \tag{A2}$$

which is equivalent to the memory kernel $\mathcal{K}(t)$ defined in (9). For the prescribed range of μ, the convergence is uniform and one has

$$\lim_{t_0\downarrow-\infty} E_\mu(-(t/\tau_f)^\mu) \ast \frac{d\mathcal{E}(t)}{dt} = \tau_f^\mu \frac{d^\mu \mathcal{E}(t)}{dt^\mu}, \tag{A3}$$

where, in the long-time limit, both the Riemann-Liouville and Caputo definitions are equivalent to the fractional derivative on the right-hand side [36]. In other words, if we assume the more general form of the SML memory decay, the stationary result is precisely that obtained in (10).

[1] A. D. Rakić, A. B. Djurišić, J. M. Elazar, and M. L. Majewski, Optical properties of metallic films for vertical-cavity optoelectronic devices, Appl. Opt. **37**, 5271–5283 (1998).

[2] J. M. Khoshman, A. Khan, and M. E. Kordesch, Amorphous hafnium oxide thin films for antireflection optical coatings, Surf. Coat. Tech. Protective Coatings and Thin Films 07, **202**, 2500–2502 (2008).

[3] C. C. Kim, J. W. Garland, H. Abad, and P. M. Raccah, Modeling the optical dielectric function of semiconductors: Extension of the critical-point parabolic-band approximation, Phys. Rev. B **45**, 11749–11767 (1992).

[4] D. Franta, D. Nečas, and I. Ohlídal, Universal dispersion model for characterization of optical thin films over a wide spectral range: Application to hafnia, Appl. Opt. **54**, 9108–9119 (2015).

[5] J. Orosco and C. F. M. Coimbra, Optical response of thin amorphous films to infrared radiation, Phys. Rev. B **97**, 094301–1–094301–10 (2018).

[6] A. Vial and T. Laroche, Description of dispersion properties of metals by means of the critical points model and application to the study of resonant structures using the FDTD method, J. Phys. D Appl. Phys. **40**, 7152–7158 (2007).

[7] K. S. Kunz and R. J. Luebbers, *The Finite Difference Time Domain Method for Electromagnetics* (CRC Press, New York, 1993).

[8] D. K. Edwards and N. Bayard De Volo, Useful Approximations for the Spectral and Total Emissivity of Smooth Bare Metals, in *Advances in Thermophysical Properties at Extreme Temperatures and Pressures*, edited by S. Gratch (ASME, New York, 1965).

[9] M. Q. Brewster, *Thermal Radiative Transfer and Properties* (J. Wiley & Sons, New York, 1992).

[10] M. Dressel and G. Grüner, *Electrodynamics of Solids: Optical Properties of Electrons in Matter* (Cambridge University Press, Cambridge ; New York, 2002).

[11] P. Drude, Optische Eigenschaften und Elektronentheorie, Ann. Phys. **319**, 936–961 (1904).

[12] L. G. Schulz, An Experimental Confirmation of the Drude Free Electron Theory of the Optical Properties of Metals for Silver, Gold, and Copper in the Near Infrared, J. Opt. Soc. Am. **44**, 540–545 (1954).

[13] S. Roberts, Interpretation of the Optical Properties of Metal Surfaces, Phys. Rev. **100**, 1667–1671 (1955).

[14] R. L. Olmon, B. Slovick, T. W. Johnson, D. Shelton, S.-H. Oh, G. D. Boreman, and M. B. Raschke, Optical dielectric function of gold, Phys. Rev. B **86**, 235147–1–235147–9 (2012).

[15] H. U. Yang, J. D'Archangel, M. L. Sundheimer, E. Tucker, G. D. Boreman, and M. B. Raschke, Optical dielectric function of silver, Phys. Rev. B. **91**, 235137–1–235137–11 (2015).

[16] S. J. Youn, T. H. Rho, B. I. Min, and K. S. Kim, Extended Drude model analysis of noble metals, Phys. Status Solidi B **244**, 1354—1362 (2007).

[17] S. R. Nagel and S. E. Schnatterly, Frequency dependence of the Drude relaxation time in metal films, Phys. Rev. B **9**, 1299–1303 (1974).

[18] D. J. Shelton, T. Sun, J. C. Ginn, K. R. Coffey, and G. D. Boreman, Relaxation time effects on dynamic conductivity of alloyed metallic thin films in the infrared band, J. Appl. Phys. **104**, 103514 (2008).

[19] H. Schulz-Baldes, Anomalous Drude Model, Phys. Rev. Lett. **78**, 2176–2179 (1997).

[20] N. V. Smith, Classical generalization of the Drude formula for the optical conductivity, Phys. Rev. B **64**, 155106–1–155106–6 (2001).

[21] J. W. Allen and J. C. Mikkelsen, Optical properties of CrSb, MnSb, NiSb, and NiAs, Phy. Rev. B. **15**, 2952–2960 (1977).

[22] D. Mayou, Generalized Drude Formula for the Optical Conductivity of Quasicrystals, Phys. Rev. Lett. **85**, 1290–1293 (2000).

[23] H. Kocer, S. Butun, Z. Li, and K. Aydin, Reduced near-infrared absorption using ultra-thin lossy metals in Fabry-Perot cavities, Sci. Rep. **5**, 8157 (2015).

[24] J. Orosco and C. F. M. Coimbra, On a causal dispersion model for the optical properties of metals, Appl. Opt. **57**, 5333–5347 (2018).

[25] M.-L. Thèye, Investigation of the Optical Properties of Au by Means of Thin Semitransparent Films, Phys. Rev. B. **2**, 3060—3078 (1970).

[26] R. A. Seban, The Emissivity of Transition Metals in the Infrared, J. Heat Transfer **87**, 173–176 (1965).

[27] J. Orosco and C. F. M. Coimbra, Variable-order modeling of nonlocal emergence in many-body systems: Application to radiative dispersion, Phys. Rev. E **98**, 032208–1–032208–14 (2018).

[28] H. Sun, W. Chen, C. Li, and Y. Chen, Fractional differential models for anomalous diffusion, Physica A **389**, 2719–2724 (2010).

[29] N. Pottier, *Nonequilibrium Statistical Physics: Linear Irreversible Processes*, Oxford graduate texts (Oxford University Press, Oxford, 2010) oCLC: 368051042.

[30] N. W. Ashcroft and N. D. Mermin, *Solid State Physics* (CBS Publishing Asia Ltd., Philadelphia, 1976).

[31] P. Drude, Zur Elektronentheorie der Metalle, Ann. Phys. **306**, 566–613 (1900).

[32] P. Drude, Zur Elektronentheorie der Metalle; II. Teil. Galvanomagnetische und thermomagnetische Effecte, Ann. Phys. **308**, 369–402 (1900).

[33] P. Drude, Zur Ionentheorie der Metalle, Phys. Z. **1**, 161–165 (1900).

[34] M.-M. Dujardin and M.-L. Thèye, Investigation of the optical properties of Ag by means of thin semi-transparent films, J. Phys. Chem. Solids **32**, 2033–2044 (1971).

[35] P. Winsemius, H. P. Lengkeek, and F. F. Van Kampen, Structure dependence of the optical properties of Cu, Ag and Au, Physica B+C **79**, 529—546 (1975).

[36] I. Podlubny, *Fractional Differential Equations*, 1st ed., Mathematics in science and engineering, Vol. 198 (Academic Press, San Diego, 1999).

[37] B. West, M. Bologna, and P. Grigolini, *Physics of Fractal Operators*, Institute for Nonlinear Science (Springer-Verlag, New York, 2003).

[38] W. Götze and P. Wölfle, Homogeneous Dynamical Conductivity of Simple Metals, Phys. Rev. B **6**, 1226–1238 (1972).

[39] P. B. Allen, Electron self-energy and generalized Drude formula for infrared conductivity of metals, Phys. Rev. B **92**, 054305 (2015).

[40] A. B. Basset, On the motion of a Sphere in a Viscous Liquid, Phil. Trans. R. Soc. Lond. A **179**, 43–63 (1888).

[41] C. F. M. Coimbra and R. H. Rangel, General solution of the particle momentum equation in unsteady Stokes flows, Journal of Fluid Mechanics **370**, 53–72 (1998).

[42] V. Lucarini, K.-E. Peiponen, J. J. Saarinen, and E. M. Vartiainen, *Kramers-Kronig Relations in Optical Materials Research*, Springer Series in Optical Sciences (Springer, Berlin, Heidelberg, 2005).

[43] A. D. Rakić, Algorithm for the determination of intrinsic optical constants of metal films: Application to aluminum, Appl. Opt. **34**, 4755–4767 (1995).

[44] S. Mirjalili, S. M. Mirjalili, and A. Lewis, Grey Wolf Optimizer, Adv. Eng. Softw. **69**, 46–61 (2014).

[45] R. Pintelon and I. Koll\'{a}r, On the Frequency Scaling in Continuous-Time Modeling, IEEE T. Instrum. Meas. **54**, 318–321 (2005).

[46] E. T. Arakawa, T. A. Callcott, and Y.-C. Chang, Beryllium (Be), in *Handbook of Optical Constants of Solids*, edited by E. D. Palik (Academic Press, Burlington, 1997) pp. 421–433.

[47] M. A. Ordal, R. J. Bell, R. W. Alexander, L. L. Long, and M. R. Querry, Optical properties of Au, Ni, and Pb at submillimeter wavelengths, Appl. Opt. **26**, 744–752 (1987).

[48] H.-J. Hagemann, W. Gudat, and C. Kunz, Optical constants from the far infrared to the x-ray region: Mg, Al, Cu, Ag, Au, Bi, C, and Al_2O_3, J. Opt. Soc. Am. **65**, 742–744 (1975).

[49] J. C. Phillips, Fermi Surface of Ferromagnetic Nickel, Phys. Rev. **133**, A1020—A1028 (1964).

[50] L. H. Jenkins, D. M. Zehner, and M. F. Chung, Characteristic energy gain and loss, double ionization, and ionization loss events in Be and BeO secondary electron spectra, Surf. Sci. **38**, 327–340 (1973).

[51] R. N. Gurzhi, A Quantum Mechanical Transport Equation for Electrons in Metals, Sov. Phys. JETP **6**, 352–358 (1958).

[52] R. N. Gurzhi, Mutual electron correlations in metal optics, Sov. Phys. JETP **8**, 673–675 (1959).

[53] R. Kohlrausch, Theorie des elektrischen Rückstandes in der Leidener Flasche, Ann. Phys. **167**, 56–82 (1854).

[54] G. Williams and D. C. Watts, Non-Symmetrical Dielectric Relaxation Behaviour Arising from a Simple Empirical Decay Function, Trans. Faraday Soc. **66**, 80–85 (1970).

[55] R. Metzler and J. Klafter, From stretched exponential to inverse power-law: Fractional dynamics, Cole–Cole relaxation processes, and beyond, J. Non-Cryst. Solids **305**, 81–87 (2002).